J. Fluid Mech. (2002), *vol.* 460, *pp.* 57–82.
DOI: 10.1017/S0022112002008066 Printed in the United Kingdom

The effect of three-dimensional obstacles on marginally separated laminar boundary layer flows

By STEFAN BRAUN AND ALFRED KLUWICK

Institute of Fluid Dynamics and Heat Transfer, Vienna University of Technology, Resselgasse 3/322, A-1040 Vienna, Austria

(Received 23 March 2001 and in revised form 30 November 2001)

We consider the steady viscous/inviscid interaction of a two-dimensional, nearly separated, boundary layer with an isolated three-dimensional surface-mounted obstacle, for example in the large Reynolds number flow around the leading edge of a slender airfoil at a small angle of attack. An integro-differential equation describing the effect of the obstacle on the wall shear stress valid within the interaction regime is derived and solved numerically by means of a spectral method, which is outlined in detail. Typical solutions of this equation are presented for different values of the spanwise width B of the obstacle including the limiting cases $B \to 0$ and $B \to \infty$. Special emphasis is placed on the occurrence of non-uniqueness. On the main (upper) solution branch the disturbances to the flow field caused by the obstacle decay in the lateral direction. Conversely a periodic flow pattern, having no decay in the spanwise direction, was found to form on the lower solution branch. These branches are connected by a bifurcation point, which characterizes the maximum (critical) angle of attack for which a solution of the strictly plane interaction problem exists. An asymptotic investigation of the interaction equation, in the absence of any obstacle, for small deviations of this critical angle clearly reflects the observed behaviour of the numerical results corresponding to the different branches. As a result we can conclude that the primarily local interaction process breaks down in a non-local manner even in the limit of vanishing (three-dimensional local) disturbances of the flow field.

1. Introduction

A systematic asymptotic analysis of Prandtl's classical boundary layer equations has shown that they inevitably lose their validity near a point of vanishing skin friction. The breakdown of the boundary layer solution occurs in two different ways characterized by the formation of a Goldstein singularity, Goldstein (1948), or of a marginal separation singularity, Ruban (1981*b*) or Stewartson, Smith & Kaups (1982), depending on the intensity of the adverse pressure gradient. As shown by Stewartson (1970), a separation singularity of the Goldstein type cannot, in general, be eliminated by means of a local interaction strategy where the displacing effect of the boundary layer affects the outer inviscid flow at leading, rather than higher, order. This is in contrast to triple-deck theory which has proven very effective in describing fully attached flows which are forced to separate over a short distance due to the occurrence of an asymptotically large pressure gradient. In contrast to the case of a Goldstein singularity, for a marginally separated singularity the solution can be continued further downstream, with the result that the wall shear stress further decreases, vanishes but

immediately recovers. Typically the intensity of the adverse pressure gradient acting on the boundary layer is measured by some controlling parameter which takes on a critical value at marginal separation. A slight increase of this parameter then is found to lead again to the occurrence of a Goldstein singularity. However, since the intensity of this singularity becomes arbitrarily small as the controlling parameter approaches its critical value it can be eliminated by locally taking into account the interaction between the viscous wall layer and the inviscid external flow region. This in turn leads to a uniformly valid description of marginally separated flows, i.e. flows which are on the verge of separation or even include short separation bubbles as demonstrated first by Ruban (1981*a*, *b*) and Stewartson *et al.* (1982).

Although a number of open problems remain, including the transition from local to global separation, a fairly complete picture of two-dimensional laminar boundary layer separation has emerged in the past three decades, see e.g. Kluwick (1998). The situation is much less satisfactory if three-dimensional flows are considered. Here only the first steps have been taken, both in flows governed by triple deck theory and marginally separated flows. In the latter case, which is of interest here, two different strategies have been applied in the past to capture three-dimensional effects. First, one can extend the analysis of Ruban and Stewartson *et al.* by considering the local properties of a three-dimensional boundary layer with (or without) additional symmetry conditions near the point (line) of vanishing wall shear, e.g. Brown (1985), Zametaev (1987), Duck (1989), and Vilenskii (1991), see also Smith (2000). But then the question arises of if and how these local structures are embedded in a global flow field, which has not been addressed in sufficient depth so far. Indeed preliminary investigations by Kluwick & Reiterer (1998) point to serious difficulties in some cases. Problems of this type are avoided in the second approach, adopted here, where one considers localized three-dimensional disturbances of an incoming two-dimensional boundary layer which is on the verge of separation caused for example by a surface-mounted obstacle. The present study therefore can be viewed as the counterpart of the triple deck study carried out by Smith, Sykes & Brighton (1977). In this connection it is of interest also to note the study by Smith & Daniels (1981) concerning flows past two-dimensional obstacles. Like the present investigation and the paper by Hackmüller & Kluwick (1989) it deals with a case where the Goldstein singularity is removable in a physically sensible fashion. In contrast to these contributions, however, the oncoming undisturbed boundary layer is assumed to be firmly attached which leads to a vastly different flow response to obstacle forcing, see also Sychev *et al.* (1998).

Following the problem formulation in § 2 an asymptotic analysis of the flow properties holding in the limit of large Reynolds numbers is carried out in § 3. Numerical solutions of the resulting nonlinear integro-differential equation for the streamwise component of the wall shear are presented in § 4. The numerical calculations indicate that the disturbances generated by a localized three-dimensional surface-mounted obstacle exhibit qualitative rather than simply quantitative differences if the incoming boundary layer is described by different branches of the solution for the case of strictly two-dimensional flow. This points to the existence of a bifurcation problem which is investigated in § 5.

2. Problem formulation

As pointed out before we consider interaction processes that are generated when a two-dimensional almost separated boundary layer on a locally flat plate encounters a three-dimensional surface-mounted obstacle, figure 1. Specific examples are provided

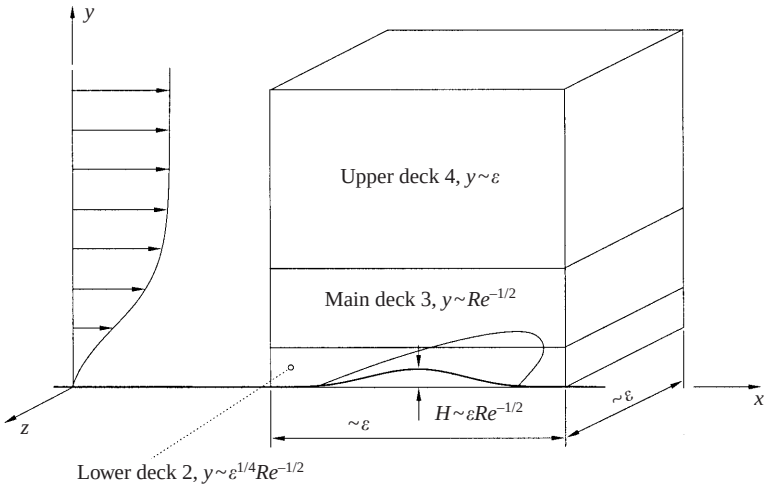

FIGURE 1. Interaction of a nearly separated two-dimensional boundary layer with a three-dimensional surface-mounted obstacle; dimensions of the various layers in the interaction regime.

by the flow in the leading edge region of a slender airfoil at a small angle of attack, Ruban (1981*a*), and by the flow past the lower wall of a channel if fluid is removed through the upper wall, Hsiao & Pauley (1994). In the first case the flow at the upper surface of the airfoil initially overexpands and is driven towards separation by the subsequent recompression. Similarly, the pressure increase associated with the removal of fluid in the second case leads to a reduction of the shear stress on the lower wall of the channel and may cause separation eventually if the suction rate is sufficiently high.

The characteristic Mach number of the flow is assumed to be small so that density changes can be neglected and the flow is taken to be laminar. Non-dimensional quantities are then introduced in the form

$$\left.\begin{aligned} (x,y,z) &= \frac{1}{\bar{L}}(\bar{x},\bar{y},\bar{z}), \quad \boldsymbol{u} = (u,v,w) = \frac{1}{\bar{u}_\infty}(\bar{u},\bar{v},\bar{w}), \\ p &= \frac{\bar{p}-\bar{p}_\infty}{\bar{\rho}_\infty \bar{u}_\infty^2}, \qquad\qquad (\tau_x,\tau_z) = \frac{\bar{L}}{\bar{\rho}_\infty \bar{\nu}_\infty \bar{u}_\infty}(\bar{\tau}_x,\bar{\tau}_z), \end{aligned}\right\} \tag{2.1}$$

where $\bar{x},\bar{z}$ and $\bar{y}$ are the coordinates in the stream-/spanwise directions and normal to the wall and $\bar{u},\bar{w}$ and $\bar{v}$ the corresponding velocity components, respectively. Furthermore, $\bar{p},\bar{\tau}_x,\bar{\tau}_z,\bar{\rho},\bar{\nu}$ and $\bar{L}$ denote the pressure, the x- and z-components of the shear stress, the density, the kinematic viscosity and a suitable reference length. The subscript ∞ indicates values of the field quantities at an appropriate reference state, e.g. the unperturbed free stream in front of an airfoil. The governing Navier–Stokes equations may then be written as

$$(\boldsymbol{u}\cdot\nabla)\boldsymbol{u} = -\nabla p + \frac{1}{Re}\Delta\boldsymbol{u}, \quad \nabla\cdot\boldsymbol{u} = 0, \tag{2.2}$$

and the no-slip condition $\boldsymbol{u} = \boldsymbol{0}$ is imposed at the solid boundary.

In the limit of large Reynolds numbers

$$Re = \frac{\bar{u}_\infty \bar{L}}{\bar{\nu}_\infty} \to \infty \tag{2.3}$$

investigated here, the interaction region of extent ε in the stream- and spanwise directions exhibits a three-tiered structure similar to that holding in two-dimensional flows, figure 1. This will be confirmed later by means of asymptotic analysis, which also yields a relationship between ε and Re.

One crucial point, to be addressed here concerns the admissible height H (non-dimensionalized with $\bar{L}$) of a localized surface-mounted obstacle, i.e. its maximum height which leaves the interaction process intact. According to slender wing theory the pressure disturbances caused by the obstacle are of $O(H/\varepsilon)$, where H characterizes the height of the obstacle. In order to affect the interaction process substantially these must be of the same order as the induced pressure perturbations, which are of $O(Re^{-1/2})$. As a result we obtain the same order of magnitude estimate

$$H \sim \varepsilon Re^{-1/2} \tag{2.4}$$

as in the case of strictly two-dimensional flows, Hackmüller & Kluwick (1989).

3. Asymptotic analysis

3.1. *Derivation of the interaction equation*

We start with the expansion of the stream function holding in the lower-deck region 2 of the interaction regime for strictly two-dimensional flows, see e.g. Ruban (1981*b*),

$$\psi_2(s_2, y_2) \sim Re^{-1/2}\left[\varepsilon^{3/4}\frac{p_{00}}{6}y_2^3 + \varepsilon^{3/2}\frac{A_1(s_2)}{2}y_2^2 + \cdots + \varepsilon^{9/4}\psi_{22}(s_2, y_2) + \cdots\right]. \tag{3.1}$$

Herein the first term represents the separation profile and A_1 represents both the lateral leading-order skin friction and the boundary layer (negative) displacement. It is influenced by the interaction process and determined by the condition that the second-order term ψ_{22} does not grow exponentially as the distance normal to the wall y_2 tends to infinity. Its asymptotic up/downstream behaviour $A_1(s_2 \to \pm\infty) \sim a_0|s_2| + b_{10}\Gamma/|s_2| + \cdots$ follows from the limiting solution of the classical boundary layer equations which exhibits the marginal separation singularity. The values of the constants a_0 and b_{10} depend on the specific problem under investigation and Γ measures the deviation of the controlling parameter α (e.g. angle of attack) from its critical value α_c characterizing the occurrence of marginal separation, $\alpha - \alpha_c = \varepsilon^2\Gamma$. The estimate of the magnitude of the secondary flow outlined below then suggests that the appropriate generalization of (3.1) for the velocity components, including the additional effect of a three-dimensional surface-mounted obstacle on the interaction process, is given by

$$\left.\begin{aligned} u_2 &\sim \varepsilon^{1/2}\frac{p_{00}}{2}y_2^2 + \varepsilon^{5/4}A_1(s_2, z_2)y_2 + \cdots + \varepsilon^2 u_{22}(s_2, y_2, z_2) + \cdots, \\ v_2 &\sim Re^{-1/2}\left[\varepsilon^{1/2}\frac{\partial}{\partial s_2}(-A_1 + p_{00}h(s_2, z_2))\frac{y_2^2}{2} + \cdots + \varepsilon^{5/4}v_{22}(s_2, y_2, z_2) + \cdots\right], \\ w_2 &\sim \varepsilon^2 w_{20}(s_2, y_2, z_2) + \cdots. \end{aligned}\right\} \tag{3.2}$$

The local coordinates s, y and z are defined by the relationships

$$x = x_0 + \varepsilon s_2, \qquad y = Re^{-1/2}(\varepsilon^{1/4}y_2 + \varepsilon h(s_2, z_2)), \qquad z = \varepsilon z_2, \tag{3.3}$$

where the index 2 indicates lower-deck quantities and Prandtl's transposition theorem was used for convenience to fulfil the no-slip condition at $y_2 = 0$. Here x_0 is the location of the marginal separation singularity according to classical boundary layer

theory and $h(s_2, z_2)$ represents the shape of the obstacle. Similarly to the case of planar flow, $A_1(s_2, z_2)$ is determined by the second-order problem. For interaction to come into play at this level of approximation the pressure gradient has to be of the form

$$\frac{\partial p_2}{\partial x} \sim p_{00} + \cdots + \varepsilon^{3/2} \frac{\partial p_2^i(s_2, z_2)}{\partial s_2} + \cdots, \qquad \frac{\partial p_2}{\partial z} \sim \varepsilon^{3/2} \frac{\partial p_2^i}{\partial z_2} + \cdots, \tag{3.4}$$

where p_{00} and p_2^i denote the prescribed pressure gradient of the inviscid flow field at x_0 and the induced pressure. Here, motivated by the results for two-dimensional flows, it has been tacitly assumed that the pressure is constant across the boundary layer. This is equivalent to assuming $\varepsilon \gg Re^{-1/2}$, that is that the streamwise extent ε of the interaction region is large compared to the boundary layer thickness, a fact which will be confirmed later. The extent of the interaction region and the leading-order magnitude of the velocity in the spanwise direction follow from the requirement of balanced inertia, pressure and friction forces in the lower deck, i.e. $u\,\partial w/\partial x \sim \partial p/\partial z \sim Re^{-1}\partial^2 w/\partial y^2 \sim \varepsilon^{3/2}$. If we require further the induced pressure gradient to be of the same magnitude in stream- and spanwise directions, it follows that $z \sim \varepsilon$ and $w \sim \varepsilon^2$.

In the main deck 3 the appropriate coordinate normal to the wall is y_3 with $y = Re^{-1/2}(y_3 + \varepsilon h(s_2, z_2))$ and the expansions for the velocity components are

$$\left.\begin{aligned} u_3 &\sim \psi_{00}'(y_3) + \varepsilon u_{31}(s_2, y_3, z_2) + \cdots, \\ v_3 &\sim Re^{-1/2}\left(v_{30}(s_2, y_3, z_2) + \psi_{00}' \frac{\partial h}{\partial s_2} + \cdots\right), \\ w_3 &\sim \varepsilon^{5/2} w_{30}(s_2, y_3, z_2) + \cdots. \end{aligned}\right\} \tag{3.5}$$

Here $\psi_{00}'(y_3)$ is the leading-order velocity profile in the streamwise direction at x_0 given from classical boundary layer theory with the asymptotic representations $\psi_{00}'(y_3 \to 0) \sim p_{00} y_3^2/2$ and $\psi_{00}'(y_3 \to \infty) \sim U_{00}$ where U_{00} denotes the velocity of the outer inviscid flow field at the solid boundary at $x = x_0$. The order of magnitude of the leading-order term in the expansion for w is the result of the balance of inertia and pressure forces in the momentum equation in the z-direction. Insertion of (3.5) into the full Navier–Stokes equations (2.2) leads to the solutions

$$\left.\begin{aligned} u_{31} &= \psi_{00}'' \frac{A_1 - p_{00} h}{p_{00}} - s_2 \frac{\mathrm{d}}{\mathrm{d}y_3}\left[\psi_{00}' \int_0^{y_3} \frac{p_{00} - \psi_{00}'''}{\psi_{00}'^2}\,\mathrm{d}\bar{y}_3\right], \\ v_{30} &= -\psi_{00}'\left[\frac{\partial}{\partial s_2}\frac{(A_1 - p_{00}h)}{p_{00}} - \int_0^{y_3} \frac{p_{00} - \psi_{00}'''}{\psi_{00}'^2}\,\mathrm{d}\bar{y}_3\right], \\ w_{30} &= -\frac{1}{\psi_{00}'} \int_{-\infty}^{s_2} \frac{\partial p_2^i}{\partial z_2}\,\mathrm{d}\bar{s}_2. \end{aligned}\right\} \tag{3.6}$$

The upper-deck '4' expansions expressed in terms of the appropriate coordinate y_4, $y = \varepsilon y_4 + Re^{-1/2}\varepsilon h$ assume the form

$$\left.\begin{aligned} u_4 &\sim U_{00} + \cdots + Re^{-1/2} u_{41}(s_2, y_4, z_2) + \cdots, \\ v_4 &\sim Re^{-1/2}\left(v_{40}(s_2, y_4, z_2) + U_{00}\frac{\partial h}{\partial s_2}\right) + \cdots, \\ w_4 &\sim Re^{-1/2} w_{40}(s_2, y_4, z_2) + \cdots, \\ \frac{\partial p_4}{\partial x} &\sim p_{00} + \cdots + Re^{-1/2}\varepsilon^{-1}\frac{\partial p_4^i(s_2, y_4, z_2)}{\partial s_2} + \cdots, \end{aligned}\right\} \tag{3.7}$$

in complete agreement with second-order boundary layer theory. Equating the pressure gradient in the upper and lower decks given by (3.4) and (3.7),

$$Re^{-1/2}\varepsilon^{-1}\frac{\partial p_4^i}{\partial s_2} \sim \varepsilon^{3/2}\frac{\partial p_2^i}{\partial s_2},$$

leads to the estimate of the extent of the interaction regime $\varepsilon \sim Re^{-1/5}$ known from investigations of planar flows. By substitution into the continuity and momentum equations one obtains

$$U_{00}u_{41} = -p_4^i, \qquad \Delta\phi = 0, \tag{3.8}$$

where $\phi(s_2, y_4, z_2)$ denotes the velocity potential defined by

$$\frac{\partial\phi}{\partial s_2} = u_{41}, \qquad \frac{\partial\phi}{\partial y_4} = v_{40}, \qquad \frac{\partial\phi}{\partial z_2} = w_{40}.$$

The solution of the Laplace equation in the half-space $y_4 > 0$ satisfying the matching condition $v_{40}(s_2, y_4 \to 0, z_2) = v_{30}(s_2, y_3 \to \infty, z_2)$ is given by

$$\phi = -\frac{1}{2\pi}\int_{-\infty}^{\infty}\int_{-\infty}^{\infty}\frac{v_{30}(\xi, y_3 \to \infty, \eta)}{[(s_2-\xi)^2 + y_4^2 + (z_2-\eta)^2]^{1/2}}\,\mathrm{d}\xi\,\mathrm{d}\eta. \tag{3.9}$$

The induced pressure is consequently deduced as

$$\begin{aligned} p_4^i(s_2, 0, z_2) = p_2^i(s_2, z_2) = -\frac{U_{00}^2}{2\pi p_{00}}\int_{-\infty}^{\infty}\int_{-\infty}^{\infty}\frac{1}{[(s_2-\xi)^2 + (z_2-\eta)^2]^{1/2}} \\ \times\frac{\partial^2}{\partial\xi^2}(A_1 - p_{00}h)\,\mathrm{d}\xi\,\mathrm{d}\eta \end{aligned} \tag{3.10}$$

using relations (3.6) and (3.8) after integration by parts, Hackmüller & Kluwick (1991), see also Kluwick, Reiterer & Hackmüller (1997). To determine the as yet unknown function A_1 we have to investigate the lower-deck equations up to second order. To simplify the boundary conditions of the resulting equations and to eliminate the various parameters entering the description of the undisturbed boundary layer we introduce

$$\left.\begin{aligned} u_{22} &= \frac{a_0^2}{24}s_2y_2^4 + \frac{3a_0^2p_{00}}{13440}y_2^8 + A_2(s_2, z_2)y_2 + \frac{A_1^2}{2p_{00}} - \frac{a_0^2}{2p_{00}}s_2^2 + U_{22}, \\ v_{22} &= -\frac{a_0^2}{120}y_2^5 + \frac{a_0^2}{p_{00}}s_2y_2 - \frac{\partial A_2}{\partial s_2}\frac{y_2^2}{2} - \frac{A_1}{p_{00}}\frac{\partial A_1}{\partial s_2}y_2 + V_{22}, \end{aligned}\right\} \tag{3.11}$$

where A_2 is unknown at this level of approximation, and the affine transformations

$$\left.\begin{aligned} s_2 &= a_0^{-2/5}p_{00}^{-1/5}U_{00}^{4/5}X, & U_{22} &= a_0^{6/5}p_{00}^{-7/5}U_{00}^{8/5}U, \\ y_2 &= a_0^{-1/10}p_{00}^{-3/10}U_{00}^{1/5}Y, & V_{22} &= a_0^{3/2}p_{00}^{-3/2}U_{00}V, \\ z_2 &= a_0^{-2/5}p_{00}^{-1/5}U_{00}^{4/5}Z, & w_{20} &= a_0^{6/5}p_{00}^{-7/5}U_{00}^{8/5}W, \\ p_2^i &= a_0p_{00}^{-1}U_{00}^2P, & A_1 &= a_0^{3/5}p_{00}^{-1/5}U_{00}^{4/5}A, \\ h &\to a_0^{3/5}p_{00}^{-6/5}U_{00}^{4/5}h, & \Gamma &\to -2^{-1}a_0^{1/5}p_{00}^{-2/5}U_{00}^{8/5}b_{10}^{-1}\Gamma. \end{aligned}\right\} \tag{3.12}$$

One finally obtains

$$\left.\begin{aligned} \frac{\partial U}{\partial X}+\frac{\partial V}{\partial Y}+\frac{\partial W}{\partial Z}&=0,\\ \frac{\partial^2 U}{\partial Y^2}-\frac{Y^2}{2}\frac{\partial U}{\partial X}-YV&=\frac{\partial P}{\partial X},\\ \frac{\partial^2 W}{\partial Y^2}-\frac{Y^2}{2}\frac{\partial W}{\partial X}&=\frac{\partial P}{\partial Z}. \end{aligned}\right\} \tag{3.13}$$

The corresponding boundary conditions and asymptotic representations of A in the limit $X\to\pm\infty$ are

$$\left.\begin{aligned} &Y=0: \quad U=X^2-A^2, \quad V=0, \quad W=0, \quad \frac{\partial V}{\partial Y}=A\frac{\partial A}{\partial X}-X,\\ &X\to\infty: \quad A^2\sim X^2-\Gamma-\frac{3\Gamma\lambda\pi}{8X^{5/2}}+\cdots,\\ &X\to-\infty: \quad A^2\sim X^2-\Gamma+\frac{2\lambda}{(-X)^{1/2}}+\cdots, \end{aligned}\right\} \tag{3.14}$$

and the requirement of no exponential growth of the field quantities for $Y\to\infty$. Using the analysis of Stewartson (1970) and the interaction relationship (3.10) one readily verifies that a solution to this system is only possible if the following solvability condition is satisfied (Hackmüller & Kluwick 1991):

$$\left.\begin{aligned} A^2-X^2+\Gamma&=\frac{\lambda}{2\pi}\int_{-\infty}^{X}\frac{\mathrm{d}t}{(X-t)^{1/2}}\int_{-\infty}^{\infty}\int_{-\infty}^{\infty}\frac{1}{[(t-\xi)^2+(Z-\eta)^2]^{1/2}}\\ &\quad\times\left(\frac{\partial^3}{\partial\xi^3}+\frac{\partial^3}{\partial\xi\partial\eta^2}\right)(A-h)\,\mathrm{d}\xi\,\mathrm{d}\eta,\\ \lambda&=\frac{(-\frac{1}{4})!}{2^{1/2}(\frac{1}{4})!}. \end{aligned}\right\} \tag{3.15}$$

As in the case of purely two-dimensional flow its solution determines the x-component of the wall shear stress

$$\tau_{wx}=Re^{11/20}\left.\frac{\partial u_2}{\partial y_2}\right|_{y_2=0}\sim Re^{3/10}a_0^{3/5}p_{00}^{-1/5}U_{00}^{4/5}A+\cdots. \tag{3.16}$$

With A and therefore also P known the crossflow velocity W can be calculated from the linear equation (3.13) by means of Fourier transformation to yield in the Fourier space

$$\begin{aligned} \tilde{W}(k,Y,Z)=&\frac{(\frac{1}{2})!\,(\frac{1}{4})!\,Y^{1/2}}{\pi^{1/2}(2\mathrm{i}\,\Omega^{1/2})^{3/4}}\left(\mathrm{e}^{-3\pi\mathrm{i}\,\mathrm{sgn}(k)/4}J_{1/4}(r)+\mathscr{H}_{-1/4}(r)\right)\\ &\times\int_{-\infty}^{\infty}\mathrm{e}^{-\mathrm{i}kX}\frac{\partial P}{\partial Z}\,\mathrm{d}X, \end{aligned} \tag{3.17}$$

where $J_\nu(s)$ and $\mathscr{H}_\nu(s)$ denote Bessel's function of the first kind and Struve's function, and $\Omega=\mathrm{i}k/8$, $r=\mathrm{i}\Omega^{1/2}Y^2$. Expansion for small Y finally leads to

$$W(X,Y\to0,Z)\sim-\frac{\mu}{\pi}\,Y\int_{-\infty}^{X}\frac{1}{(X-t)^{3/4}}\frac{\partial P}{\partial Z}\,\mathrm{d}t+O(Y^2), \quad \mu=\frac{(\frac{1}{2})!\,(-\frac{1}{4})!}{2^{1/4}}. \tag{3.18}$$

From this result one immediately derives the leading-order term of the wall shear in the spanwise direction,

$$\tau_{wz} = Re^{11/20}\frac{\partial w_2}{\partial y_2}\bigg|_{y_2=0} \sim Re^{3/20}a_0^{13/10}p_{00}^{-11/10}U_{00}^{7/5}\left(-\frac{\mu}{\pi}\int_{-\infty}^{X}\frac{1}{(X-t)^{3/4}}\frac{\partial P}{\partial Z}\,\mathrm{d}t + \cdots\right) \tag{3.19}$$

whose order of magnitude is seen to be much smaller than that of the wall shear in the streamwise direction.

The interaction equation (3.15) will be solved numerically using a spectral method. To this end it is useful to decompose the wall shear and the geometry of the obstacle in the form

$$A(X,Z) = A_\infty(X) + A_1(X,Z), \quad h(X,Z) = h_\infty(X) + h_1(X,Z), \tag{3.20}$$

where the subscripts ∞ and 1 refer to two-dimensional and three-dimensional contributions, respectively. As a result one obtains

$$A_\infty^2 - X^2 + \Gamma = \lambda\int_X^\infty \frac{(A_\infty - h_\infty)''}{(\xi - X)^{1/2}}\,\mathrm{d}\xi, \quad A_\infty(X \to \pm\infty) \sim |X| + \cdots \tag{3.21}$$

and

$$\left.\begin{aligned} 2A_\infty A_1 + A_1^2 = {} & \frac{\lambda}{2\pi}\int_{-\infty}^{X}\frac{\mathrm{d}t}{(X-t)^{1/2}}\int_{-\infty}^{\infty}\int_{-\infty}^{\infty}\frac{1}{[(t-\xi)^2 + (Z-\eta)^2]^{1/2}} \\ & \times\left(\frac{\partial^3}{\partial\xi^3} + \frac{\partial^3}{\partial\xi\partial\eta^2}\right)(A_1 - h_1)\,\mathrm{d}\xi\,\mathrm{d}\eta, \\ & A_1(X \to \pm\infty, Z) \to 0. \end{aligned}\right\} \tag{3.22}$$

Equation (3.21) is the solvability condition for planar flow known from previous work, Hackmüller & Kluwick (1989), whose solution A_∞ is prescribed in (3.22) to determine the three-dimensional contribution A_1 to the wall shear A.

3.2. *The limiting cases of slender and wide obstacles*

The solvability condition (3.15) or its equivalent form given by equations (3.21) and (3.22) has to be solved numerically in general. Before doing so it is, however, useful to consider the limiting cases of slender and wide surface-mounted obstacles where considerable simplifications are possible. The resulting approximations are not only useful insofar as they establish connections to earlier studies dealing with quasi-three-dimensional flows but also as a means to check the numerical scheme used to investigate obstacles whose extent in the spanwise direction measured by the parameter B is of order one. In both cases $B \ll 1$ and $B \gg 1$ the z-coordinate has to be stretched appropriately

$$\hat{Z} = \frac{Z}{B}. \tag{3.23}$$

In the limit $B \to 0$, which will be considered first, integration by parts with respect to ξ of the part containing the third ξ-derivative and with respect to $\hat{\eta}$ of the remaining part and substitution of the variable $s = (t-\xi)/(\hat{Z} - \hat{\eta})$ in place of ξ leads to the

following form of the term on the right-hand side of equation (3.22):

$$\frac{\lambda}{2\pi}\int_{-\infty}^{X}\frac{\mathrm{d}t}{(X-t)^{1/2}}\int_{-\infty}^{\infty}\int_{-\infty}^{\infty}\frac{B}{(s^2+B^2)^{3/2}}\frac{\mathrm{sgn}(\hat{Z}-\hat{\eta})}{(\hat{Z}-\hat{\eta})^2}$$
$$\times\left(\frac{\partial^2}{\partial s\partial\hat{\eta}}+\frac{1}{(\hat{Z}-\hat{\eta})}\frac{\partial}{\partial s}\right)\left(\hat{A}_1(t-(\hat{Z}-\hat{\eta})s,\hat{\eta})-\hat{h}_1(t-(\hat{Z}-\hat{\eta})s,\hat{\eta})\right)\mathrm{d}\hat{\eta}\mathrm{d}s.$$

Making use of the relationship

$$\lim_{B\to 0}\frac{B^2}{2}\int_{-\infty}^{\infty}\frac{\varphi(s)}{(s^2+B^2)^{3/2}}\,\mathrm{d}s=\varphi(0)$$

holding for continuously differentiable functions φ with bounded first derivatives, one then obtains the approximate version of equation (3.22)

$$2A_\infty\hat{A}_1+\hat{A}_1^2\sim\frac{\lambda}{B\pi}\int_{-\infty}^{X}\frac{\mathrm{d}t}{(X-t)^{1/2}}\frac{\partial}{\partial t}\int_{-\infty}^{\infty}\frac{1}{|\hat{Z}-\hat{\eta}|}\left(\frac{\partial}{\partial\hat{\eta}}+\frac{1}{\hat{Z}-\hat{\eta}}\right)(\hat{A}_1-\hat{h}_1)\,\mathrm{d}\hat{\eta}+O(1)\tag{3.24}$$

with $A_1(X,Z)=\hat{A}_1(X,\hat{Z})$ and $h_1(X,Z)=\hat{h}_1(X,\hat{Z})$, from which it may be inferred that

$$A\sim A_\infty+h_1+O(B),\quad B\to 0.\tag{3.25}$$

At leading order, therefore, the perturbation displacement thickness A simply equals the function $A_\infty+h_1$ which characterizes the sum of the contribution of the planar problem and the shape of the surface-mounted obstacle.

To simplify the description of flows past wide obstacles the integration variable $\zeta=B(\hat{Z}-\hat{\eta})$ is introduced. Rewriting the term within brackets on the right-hand side of equation (3.15) in the form

$$\left(\frac{\partial^2}{\partial\xi^2}+\frac{1}{B^2}\frac{\partial^2}{\partial(\hat{Z}-\zeta/B)^2}\right)\hat{A}(\xi,\hat{Z}-\zeta/B)=\frac{\partial^2}{\partial\xi^2}\hat{A}(\xi,\hat{Z})+O(B^{-1})$$

then suggests the approximation

$$\hat{A}^2-X^2+\Gamma\sim\lambda\int_X^{\infty}\frac{1}{(\xi-X)^{1/2}}\frac{\partial^2}{\partial\xi^2}(\hat{A}-\hat{h})\,\mathrm{d}\xi+O(B^{-2}),\quad B\to\infty.\tag{3.26}$$

The lateral distance Z enters the quasi-two-dimensional form of the solvability condition for A as a parameter only. Solutions to this equation can thus be constructed from the results for two-dimensional flows (cf. equation (3.21)) as pointed out by Hackmüller & Kluwick (1991). The limiting solution (3.25) and that of equation (3.26) are depicted in figures 6 and 7.

4. Numerical analysis

4.1. *Numerical scheme*

Applying a Fourier transform with respect to the spanwise coordinate Z, namely

$$\tilde{f}(X,k)=\int_{-\infty}^{\infty}f(X,Z)\,\mathrm{e}^{-\mathrm{i}kZ}\,\mathrm{d}Z,\tag{4.1}$$

to equation (3.22), making use of the convolution theorem and assuming that the surface-mounted obstacle is symmetrical with respect to the z-axis yields

$$2A_\infty\tilde{A}_1+\int_{-\infty}^{\infty}A_1^2\,\mathrm{e}^{-\mathrm{i}kZ}\,\mathrm{d}Z=\frac{\lambda}{\pi}\int_{-\infty}^{X}\frac{\mathrm{d}t}{(X-t)^{1/2}}\int_{-\infty}^{\infty}K_0(|t-\xi|k)\times\left(\frac{\partial^3}{\partial\xi^3}-k^2\frac{\partial}{\partial\xi}\right)(\tilde{A}_1-\tilde{h}_1)\,\mathrm{d}\xi.$$

Here $K_0(s)$ denotes the modified Bessel function of zeroth order, Abramowitz & Stegun (1970). Integration by parts with respect to ξ and extracting the singular part of the modified Bessel function $K_1(s)$ leads to

$$2A_\infty\tilde{A}_1+\int_{-\infty}^{\infty}A_1^2\,\mathrm{e}^{-\mathrm{i}kZ}\,\mathrm{d}Z=\lambda\int_{X}^{\infty}\frac{1}{(\xi-X)^{1/2}}\left(\frac{\partial^2}{\partial\xi^2}-k^2\right)(\tilde{A}_1-\tilde{h}_1)\,\mathrm{d}\xi+\frac{\lambda k}{\pi}\int_{-\infty}^{X}\frac{\mathrm{d}t}{(X-t)^{1/2}}\int_{-\infty}^{\infty}\mathscr{K}_1(|t-\xi|k)\,\mathrm{sgn}(\xi-t)\left(\frac{\partial^2}{\partial\xi^2}-k^2\right)(\tilde{A}_1-\tilde{h}_1)\,\mathrm{d}\xi,\quad(4.2)$$

with

$$\mathscr{K}_1(s)=K_1(s)-\frac{1}{s}.\quad(4.3)$$

Exchanging the sequence of integration of the second term on the right-hand side of equation (4.2) finally results in

$$2A_\infty\tilde{A}_1+\int_{-\infty}^{\infty}A_1^2\,\mathrm{e}^{-\mathrm{i}kZ}\,\mathrm{d}Z=\lambda\int_{X}^{\infty}\frac{1}{(\xi-X)^{1/2}}\left(\frac{\partial^2}{\partial\xi^2}-k^2\right)(\tilde{A}_1-\tilde{h}_1)\,\mathrm{d}\xi-\lambda\sqrt{k}\int_{-\infty}^{\infty}G((\xi-X)k)\left(\frac{\partial^2}{\partial\xi^2}-k^2\right)(\tilde{A}_1-\tilde{h}_1)\,\mathrm{d}\xi,\quad(4.4)$$

where the function G is defined by

$$G(s)=-\frac{2}{\pi}\int_0^{\infty}\mathscr{K}_1(|s+v^2|)\,\mathrm{sgn}(s+v^2)\,\mathrm{d}v.\quad(4.5)$$

Fast numerical calculation of $G(s)$ for large arguments is achieved by using its asymptotic representations. Applying Watson's lemma to (4.5) we obtain

$$G(s\to\infty)\sim\frac{1}{\sqrt{s}}+O\left(\frac{\mathrm{e}^{-s}}{\sqrt{s}}\right).\quad(4.6)$$

Straightforward application of Watson's lemma to expression (4.5) does not lead to the correct asymptotic behaviour for $s\to-\infty$. However, comparison of the Fourier-transformed equation (3.24) and (4.4) in the limit $X\to\infty$ and $k\to\infty$,

$$-\int_{-\infty}^{X}\frac{1}{(X-t)^{1/2}}\frac{\partial}{\partial t}(\tilde{A}_1-\tilde{h}_1)\,\mathrm{d}t\sim k^{3/2}\int_{-\infty}^{\infty}G((\xi-X)k)(\tilde{A}_1-\tilde{h}_1)\,\mathrm{d}\xi$$

yields the desired result

$$G(s\to-\infty)\sim\frac{1}{2(-s)^{3/2}}+O((-s)^{-7/2})\quad(4.7)$$

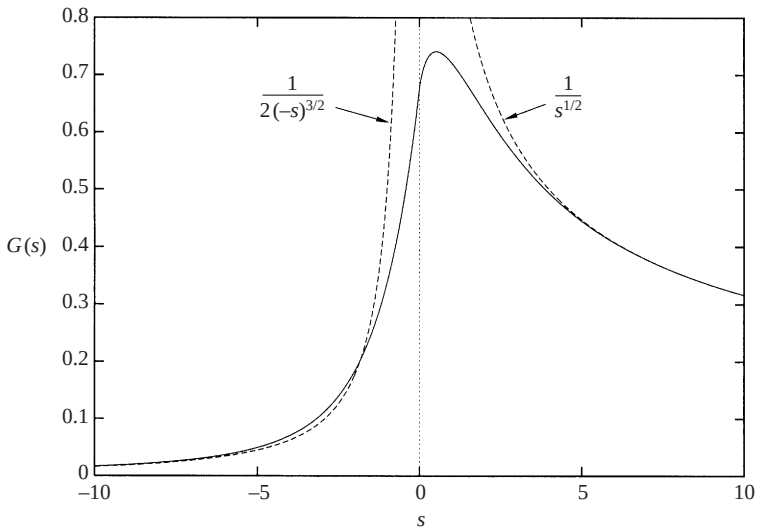

FIGURE 2. $G(s)$ and its asymptotes, equations (4.5), (4.6) and (4.7).

after integration by parts. An alternative approach to (4.7) is to introduce $\omega = (-s)^{1/2}v$ as a new integration variable so that

$$G(s \to -\infty) = -\frac{2(-s)^{1/2}}{\pi}\int_0^\infty \left[-\frac{1}{-s(\omega^2-1)} + K_1(-s|\omega^2-1|)\,\mathrm{sgn}(\omega^2-1)\right]\mathrm{d}\omega$$

$$\sim -\frac{2}{\pi(-s)^{1/2}}\int_0^\infty \left[K_1\left(2q+\frac{q^2}{(-s)}\right) - K_1\left(2q-\frac{q^2}{(-s)}\right)\right]\mathrm{d}q + \cdots$$

on writing $\omega = 1 - q/(-s)$ for $\omega < 1$ and $\omega = 1 + q/(-s)$ for $\omega > 1$. Taylor series expansion of the modified Bessel function immediately yields

$$G(s \to -\infty) \sim -\frac{4}{\pi(-s)^{3/2}}\int_0^\infty q^2 K_1'(2q)\,\mathrm{d}q + \cdots = \frac{1}{2(-s)^{3/2}} + \cdots.$$

A graphical representation of G is given in figure 2.

The integrals in equations (3.21) and (4.4) are split into two or three parts,

$$\int_X^\infty \cdot\,\mathrm{d}\xi = \left(\int_X^{X_N} + \int_{X_N}^\infty\right)\cdot\,\mathrm{d}\xi, \quad \int_{-\infty}^\infty \cdot\,\mathrm{d}\xi = \left(\int_{-\infty}^{X_0} + \int_{X_0}^{X_N} + \int_{X_N}^\infty\right)\cdot\,\mathrm{d}\xi. \tag{4.8}$$

The calculation domain in the streamwise direction $X \in [X_0, X_N]$ used in the numerical scheme is chosen to be large enough so that the contributions of the outside range can be calculated analytically using the asymptotic representations of $A_\infty(X \to \pm\infty)$, (3.14) and $A_1(X \to \pm\infty, Z)$ whose asymptotic behaviour is determined by the shape of the obstacle $h_1(X, Z)$. The remaining integrals in (4.8) are treated numerically. To this end the calculation domain is divided into N equidistant cells with a mesh size of $\Delta X = (X_N - X_0)/N$ and X discretized by $X_i = X_0 + i\Delta X$, $i = (0, \ldots, N)$. Assuming sufficiently smooth solutions of the integral equations, a linear approximation of the form

$$f(\xi) = f_j + \frac{f_{j+1} - f_j}{\Delta X}(\xi - \xi_j) + O(\Delta X^2), \quad f_j = f(\xi_j), \quad \xi \in [\xi_j, \xi_{j+1}]$$

leads to

$$\int_{X_i}^{X_N} \frac{f(\xi)}{(\xi - X_i)^{1/2}}\,\mathrm{d}\xi$$

$$\approx \frac{\sqrt{\Delta X}}{3}\left[4f_i + 4\sum_{j=i+1}^{N-1}((j-i+1)^{3/2} - 2(j-i)^{3/2} + (j-i-1)^{3/2})f_j\right.$$

$$\left. +(4(N-i-1)^{3/2} + 2(3-2N+2i)(N-i)^{1/2})f_N\right],\ i = (0,\ldots,N-1) \tag{4.9}$$

after exact integration of the kernel function. Similar considerations lead to

$$\int_{X_0}^{X_N} G((\xi - X_i)k)f(\xi)\,\mathrm{d}\xi \approx \frac{\Delta X}{2}\left[\sum_{j=1}^{N-1}(G_{j+1,i} + G_{j-1,i})f_j + G_{1,i}f_0 + G_{N-1,i}f_N\right] \tag{4.10}$$

with $G_{j,i} = G((j-i)\Delta Xk)$. Derivatives were replaced by second-order-accurate central differencing formulas and the calculation domain in the Fourier space was limited to $[0, M\Delta k]$. Here $M+1$ is the number of grid points, $\Delta k = \pi/Z_M$ the step size of the wavenumber k and $[0, Z_M]$ the corresponding domain in the spanwise direction of the physical space. Assuming obstacles which are symmetrical with respect to the z-axis, i.e. $A(X,Z) = A(X,-Z)$, it is sufficient to perform a cosine Fourier transform, having the symmetrical discrete form

$$\tilde{f}(p\Delta k) = \sqrt{\frac{2}{M}}\left[\frac{f_0}{2} + \sum_{j=1}^{M-1} f_j \cos\frac{\pi pj}{M} + (-1)^p\frac{f_M}{2}\right], \quad p = 0,\ldots,M, \tag{4.11}$$

so that double application of (4.11) generates the primary quantity $f_p = f(pZ_M/M)$.

It should be noted that the discretization of the integrals of (4.4) with respect to the streamwise coordinate by means of the trapezium rule after a transformation of the integration variable to avoid the singularity of the kernel (scheme II of Stewartson *et al.* (1982)) is not sufficient to prevent unphysical oscillations of the solution on the calculation grid. However, the stepwise linear approximation of the solution A described above leads to satisfactory smooth results.

To obtain $A_1(X,Z)$ for a specific value of Γ the corresponding solution $A_\infty(X)$ of equation (3.21) is substituted into (4.4). $A_1(X,Z)$ then is written in the form $A_1^{(n+1)} = A_1^{(n)} + \Delta A_1^{(n)}$ and an iteration procedure is applied to equation (4.4) which then symbolically is of the form

$$\boldsymbol{M}_1\Delta\tilde{A}_1^{(n)} = \boldsymbol{M}_2\tilde{A}_1^{(n)} - \left(A_1^{(n)2}\right)^{\sim} + \text{obstacle contributions} + \text{asymptotic parts} \tag{4.12}$$

after linearization with respect to the deviation $\Delta A_1^{(n)}$. Here n denotes the nth iteration and $\boldsymbol{M}_1$, $\boldsymbol{M}_2$ are matrices fixed by the numerical scheme. In each iteration step the linear system (4.12) is solved for $\Delta\tilde{A}_1^{(n)}$ and back and forth Fourier transformation is used to update $A_1^{(n)}$ and to calculate the first and second terms on the right-hand side from the previous step. The iteration process is continued until the discrete $\mathscr{L}_2$ norm

X_0	X_N	N	Z_M	M	ϵ
$-(10–5)$	7–15	200–400	$\gtrapprox 30B$	100–1000	10^{-6}

TABLE 1. Typical parameter values in the numerical scheme.

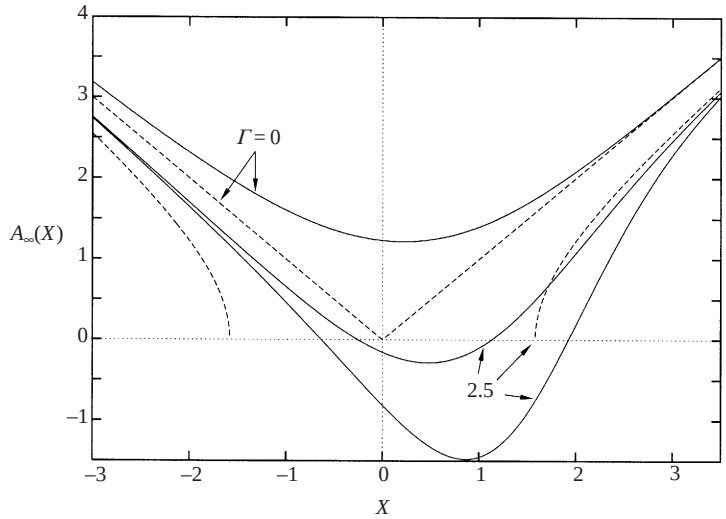

FIGURE 3. Wall shear distributions and non-uniqueness in the case of two-dimensional flow past a locally flat wall (equation (3.21) with $h_\infty = 0$), Ruban (1981*b*), Stewartson *et al.* (1982). Dashed lines represent corresponding solutions of the classical boundary layer equations (marginal separation and weak Goldstein singularity).

is less than some certain value ϵ:

$$\left[\frac{(X_N - X_0)}{N}\frac{Z_M}{M}\sum_{i=0}^{N}\sum_{p=0}^{M}(A_1^{(n+1)}(X_i, Z_p) - A_1^{(n)}(X_i, Z_p))^2\right]^{1/2} < \epsilon.$$

Here we have used the notation $Z_p = pZ_M/M$. The initial values $A_1^{(0)}(X_i, Z_p)$ are chosen to be zero and an under-relaxation factor of about 0.6–0.9 is used to update $A_1^{(n)}$ in the iteration process. Numerical parameters determining the calculation domain and the discretization are summarized in table 1.

4.2. *Numerical results*

Before turning to a discussion of three-dimensional flows it is useful to recall some results for planar flows past a locally flat wall, equation (3.21) with $h_\infty = 0$. First, interaction delays separation as can be seen from figure 3 for $\Gamma = 0$. Secondly, there exists an upper bound Γ_c of Γ, up to which the theory of marginally separated flows holds. For $\Gamma > \Gamma_c$, where $\Gamma_c \approx 2.66$, the interactive strategy breaks down and (real) solutions of the integral equation (3.21) do not exist, Chernyshenko (1985), indicating a global change of the flow field presumably associated with a rapid transition from a short separation bubble to a much longer one. For further comments on the phenomenon of short bubble bursting the reader is referred to Sychev *et al.* (1998). Finally, the solutions of the interaction equation are non-unique within the range $0 < \Gamma < \Gamma_c$, figure 3. The usual way to express this non-uniqueness investigated

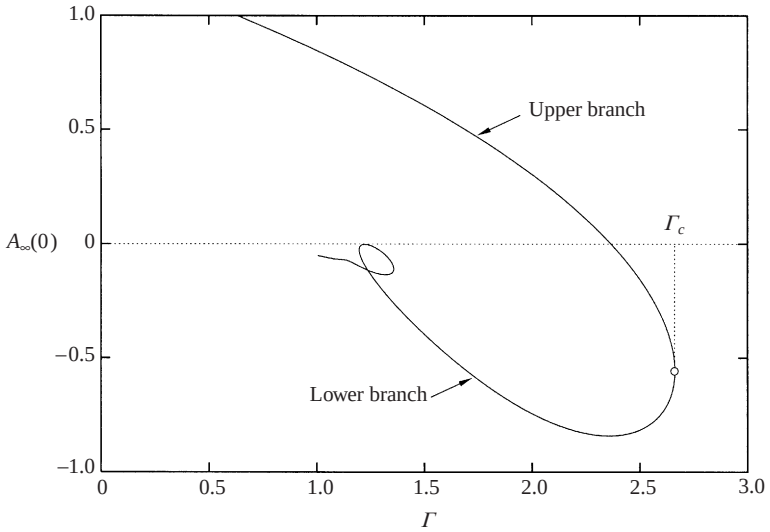

FIGURE 4. Non-uniqueness of the planar boundary layer flow ($h_\infty \equiv 0$), Stewartson *et al.* (1982).

in detail by Stewartson *et al.* (1982) and Brown & Stewartson (1983) is to plot the value of the wall shear A_∞ at $X = 0$ versus Γ. The resulting diagram is depicted in figure 4.

As a representative example of solutions including three-dimensional effects we consider isolated surface-mounted obstacles of the form

$$h_1(X,Z) = H(1-X^2)^3\,\theta(1-|X|)\,\mathrm{e}^{-(Z/B)^2}, \tag{4.13}$$

figure 5. Here $H = h_1(0,0)$ is the maximum height of the obstacle, B a measure of its width and $\theta(X)$ denotes Heaviside's step function. The special choice (4.13) leads to the asymptotic representations

$$\tilde{A}_1(X \to \pm\infty, k) \sim \mp\frac{16\sqrt{\pi}}{35}\lambda H B k^{5/2}\,\mathrm{e}^{-(kB/2)^2}\,\frac{G(-kX)}{X} + \cdots \tag{4.14}$$

which can be derived from (4.4) in the sense of the first step of a successive approximation applied to $\tilde{A}_1$, i.e. by neglecting $\tilde{A}_1$ and A_1 in the integral terms of equation (4.4). Results for the wall shear distribution $A(X,Z)$ in the plane of symmetry $Z = 0$ and in the lateral direction at $X = 0$ are shown in figures 6 and 7 for different values of B and fixed values of Γ and H. Specifically we consider a hill with $H = 4$ and the case of an unperturbed boundary layer which is at the verge of separation but still attached, $\Gamma = 1$. For large values of B, the numerical solutions of the interaction equation (3.15) are found to be in excellent agreement with the solution of equation (3.26) for quasi-two-dimensional flows obtained by Hackmüller & Kluwick (1991), which predict the formation of a separation zone on the leeward side of the hill. As the lateral extent B of the hill decreases, the axial component A of the wall shear stress is seen to increase. As a consequence, the separated flow region shrinks and eventually vanishes. Finally for $B \to 0$ the numerical solution is seen to approach the asymptotic result (3.25). It turned out that the value $B \approx 0.1$ is the most sensitive one concerning the requirements on the parameters of the numerical scheme. The reason for this fact is the weaker decay behaviour of the solution A_1 for $X \to \infty$ and $Z/B \to \infty$ as can be seen from figures 6 and 7, respectively.

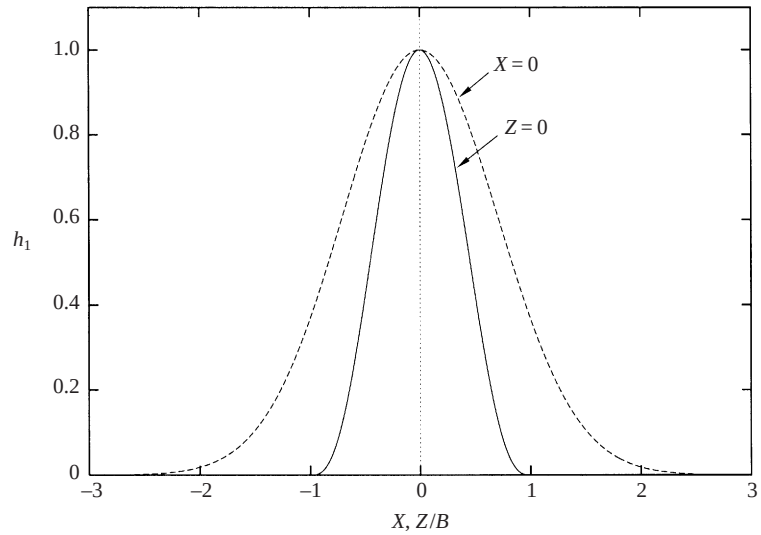

FIGURE 5. Vertical sections of the shape $h_1(X, Z)$ of the obstacle according to (4.13) with $H = 1$ in the streamwise ($Z = 0$) and spanwise ($X = 0$) directions.

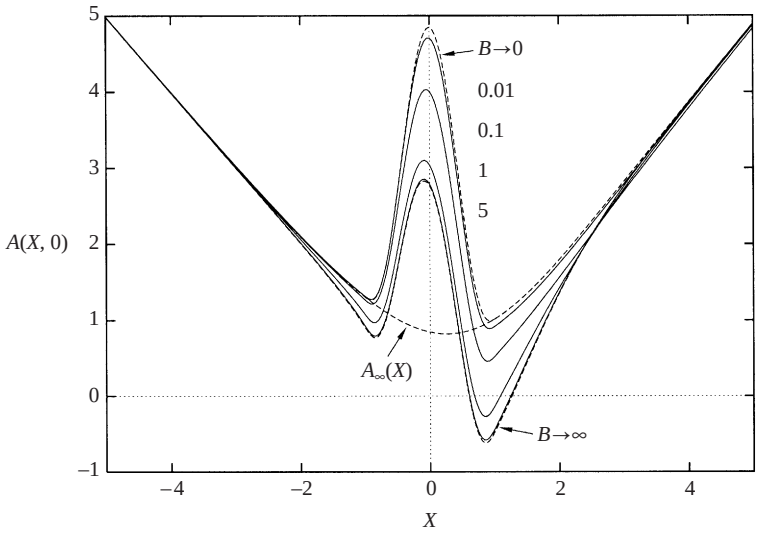

FIGURE 6. Typical solutions of (3.15) in the plane of symmetry $Z = 0$ for $\Gamma = 1$ (upper branch) for the hill geometry (4.13) and various values of B and $H = 4$. Dashed lines denote the asymptotic limits of the solutions for $B \to 0$, (3.25), and $B \to \infty$, (3.26), as well as the solution $A_\infty(X)$ of the plane problem without hill.

The effects of a dent with $H = -1.5$ on an attached boundary layer characterized by $\Gamma = 2$ are considered in figures 8 and 9. Like figures 6 and 7 the numerical results support the analytical prediction (3.25) holding in the limit $B \to 0$. However, the dent is seen to generate a more pronounced separated flow region. Also, in contrast to figures 6 and 7 a strictly two-dimensional solution $B \to \infty$ does not exist. As a consequence, interacting flows past a localized three-dimensional dent are possible only up to a maximum value of $B \lesssim 3$. Taking into account the results obtained by Hackmüller & Kluwick (1989) the following qualitative picture of the flow past a

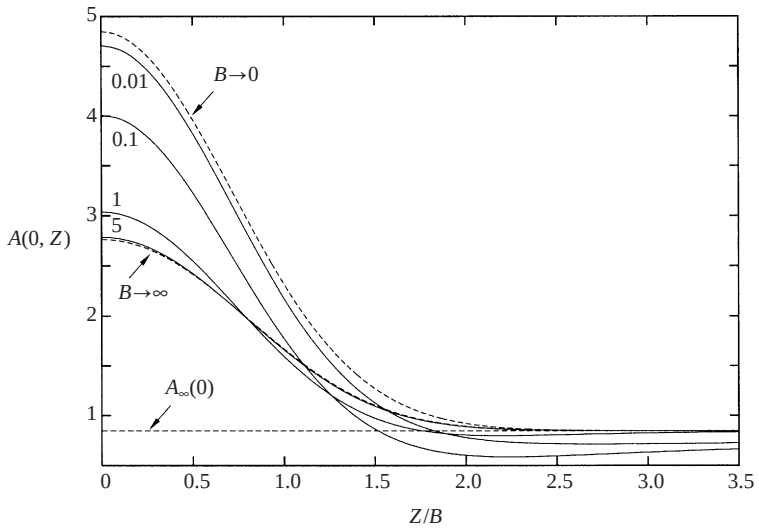

FIGURE 7. Decay behaviour of typical solutions of (3.15) for $\Gamma = 1$ (upper branch) in the spanwise direction for the hill geometry (4.13) and various values of B and $H = 4$. Dashed lines denote the asymptotic limits of the solutions for $B \to 0$, (3.25) and $B \to \infty$, (3.26) as well as the value $A_\infty(0)$ of the plane problem without hill.

three-dimensional obstacle placed into an almost separated boundary layer emerges. In the case of strictly planar flows $B = \infty$ solutions of the interaction equation exist (if they exist at all) for a limited range of the parameter H characterizing the height of the obstacle only. A simple argument supporting this finding results from the observation that the terms on the right-hand side of equation (3.15) which depend on the shape of the obstacle can be evaluated once $h(X)$ is given, effectively leading in turn to a modification of the parameter Γ. The non-existence of solutions for flows past locally plane walls if $\Gamma > \Gamma_c$ and for flows past surface-mounted obstacles if H exceeds a critical value, therefore, appear to be closely related. The same argument also applies to the case of three-dimensional flows and numerical calculations indicate that the range of the parameter H for which solutions of equation (3.15) exists expands with decreasing values of B. Indeed the asymptotic result (3.25) suggests that solutions for $|H| \to \infty$ may exist in the limit $B \to 0$ but this has yet to be investigated.

Like the case of two-dimensional flows past locally flat walls where interactive solutions do not exist if $\Gamma > \Gamma_c$ the non-existence of solutions if $B > B_c$ or $|H| > H_c$ is taken as an indication that a significant change of the flow field which cannot be captured by the present theory will take place if the parameters B and $|H|$ increase beyond critical values B_c and H_c.

Three-dimensional disturbances of a planar flow characterized by a lower-branch solution $\Gamma = 2.03$ generated by a dent with $H = -0.25$ are displayed in figures 10 and 11. Here the unperturbed flow exhibits an extended separation zone which is only slightly modified by the dent of relatively small depth. Nevertheless, the approach to the limiting results for $B \to 0$ and $B \to \infty$ is clearly visible. According to figures 6–9 localized surface-mounted obstacles generate disturbances of two-dimensional upper-branch solutions which are localized in the stream- and spanwise direction as one would expect intuitively. In sharp contrast, the disturbances generated in a flow characterized by a lower-branch solution are seen to set up a flow field which is periodic in the lateral direction and extends up to $Z \to \pm\infty$. This interesting

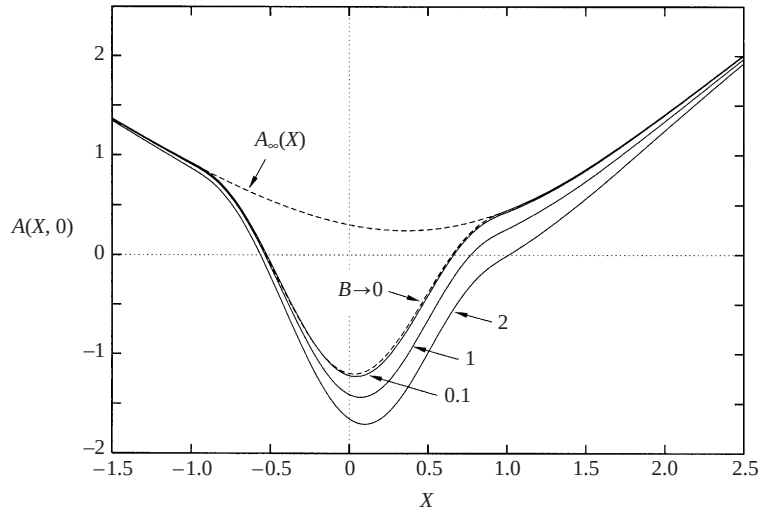

FIGURE 8. Solutions of (3.15) for $\Gamma = 2$ and a dent according to (4.13) for $H = -1.5$ and various values of B (upper branch). No solutions can be found for $B \gtrsim 3$.

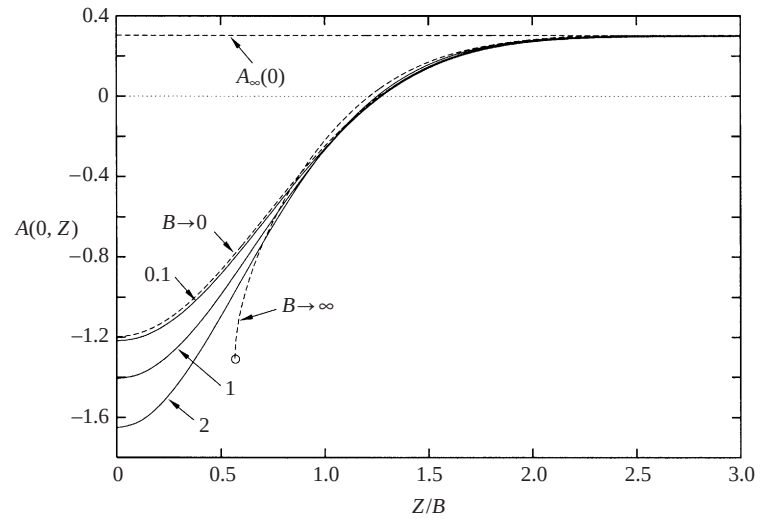

FIGURE 9. Decay behaviour in the lateral direction of the solutions of (3.15) for $\Gamma = 2$ and a dent according to (4.13) for $H = -1.5$ and various values of B (upper branch). No solution can be found for $B \gtrsim 3$. The open circle denotes the limiting solution of the planar problem with a dent of maximum possible depth $H = -1.09$.

result was checked carefully by changing the step size and lateral extent of the computational domain. The numerical experiments indicate that the results shown in figure 11 are reliable both for the wavelength and the amplitude of the periodic pattern. Furthermore the numerical calculations show that the wavelength is almost independent of B while the amplitude tends to zero for $B \to 0$ and $B \to \infty$ in order to recover the asymptotic results holding in these limits.

In order to shed further light on the qualitatively different behaviour of two-dimensional upper- and lower-branch solutions when subjected to localized three-dimensional surface-mounted obstacles we now focus on the question of what happens

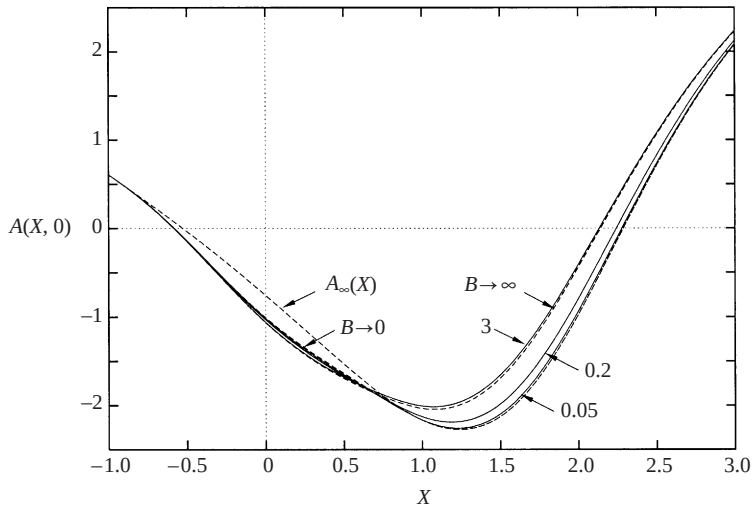

FIGURE 10. Solutions of (3.15) for $\Gamma = 2.03$ and a dent according to (4.13) for $H = -0.25$ and various values of B (lower branch).

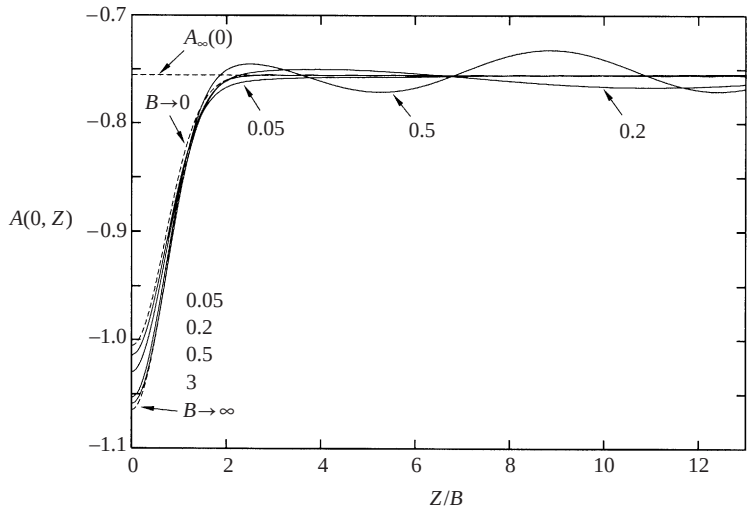

FIGURE 11. Decay behaviour in the lateral direction of the solutions of (3.15) for $\Gamma = 2.03$ and a dent according to (4.13) for $H = -0.25$ and various values of B (lower branch).

to the three-dimensional solution if Γ_c is approached moving along the upper branch of the $A_\infty(0)$-Γ curve. To obtain some preliminary insight into the flow behaviour, we consider the dependence of the value of the wall shear A in the streamwise direction at $X = 0$ on spanwise coordinate Z in more detail. Two remarkable observations were made during the numerical investigation: first, the maximum possible hill height H tends to zero in the limit $\Delta\Gamma = \Gamma_c - \Gamma \to 0$, in other words the three-dimensional solution coincides with the plane one for $\Gamma = \Gamma_c$. Secondly, as can be seen from figure 12 for fixed H and B the influence of the obstacle extends to increasing values of Z for decreasing values of $\Delta\Gamma$. In agreement with the results depicted in figure 11 a completely different behaviour of the three-dimensional solutions was found at the lower branch. A periodic flow pattern appears without decay in the lateral direction,

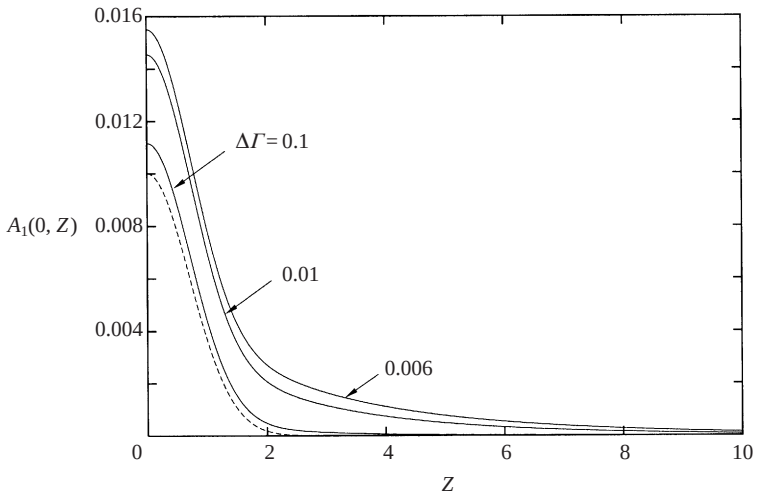

FIGURE 12. Numerical solutions of (3.15) for the upper branch near Γ_c for a hill shape according to (4.13) with $H = 0.01$ and $B = 1$ (dashed line).

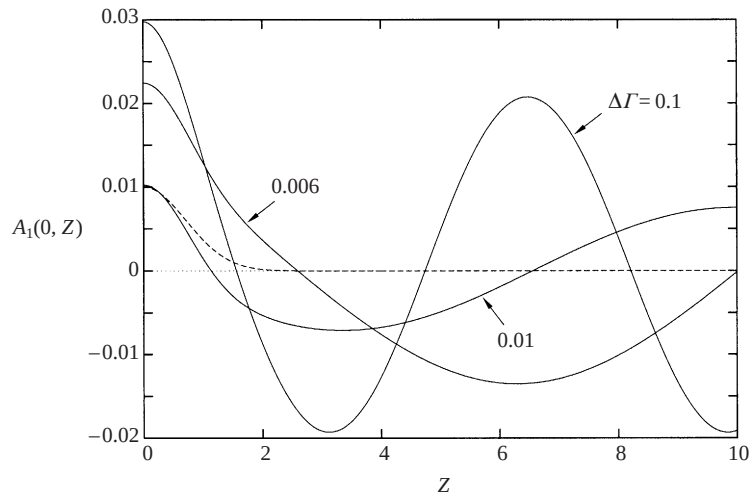

FIGURE 13. Numerical solutions of (3.15) for the lower branch near Γ_c for a hill shape according to (4.13) with $H = 0.01$ and $B = 1$ (dashed line).

figure 13. The wavelength and amplitude of the shear stress distribution depends on the value of $\Delta\Gamma$ and is influenced by the geometry of the obstacle. Combining these observations we conclude that the solution of the problem of interest bifurcates as we pass through Γ_c moving from the upper to the lower branch of the $A_\infty(0), \Gamma$ curve.

5. Bifurcation problem – three-dimensional solutions without an obstacle

5.1. *Asymptotic analysis for* $\Delta\Gamma \to 0$

To simplify the analysis of the bifurcation problem detected during the numerical investigation we seek non-trivial three-dimensional solutions of the interaction equation (3.15) for a locally flat wall, $h(X, Z) = h_\infty(X) \equiv 0$. The difference $\Gamma_c - \Gamma = \Delta\Gamma$ then enters as the only perturbation parameter. The parabolic shape of the $A_\infty(0), \Gamma$

curve near Γ_c, figure 4, then suggests the following expansions for $\Delta\Gamma \to 0$:

$$A(X,Z;\Delta\Gamma) \sim A_{\infty c}(X) + \sqrt{\Delta\Gamma}\, a_1(X,\Delta\Gamma^{1/4}Z) + \Delta\Gamma\, a_2(X,\Delta\Gamma^{1/4}Z) + \cdots, \tag{5.1}$$

where the coordinate in the spanwise direction is suitably rescaled with respect to $\Delta\Gamma$. The leading-order term $A_{\infty c}(X)$ in the expansion (5.1) of the wall shear distribution is the solution for strictly planar flow with $\Gamma = \Gamma_c$. Insertion of (5.1) into (3.15) after performing integration by parts with respect to ξ finally leads to the staggered system

$$O(1): \quad A_{\infty c}^2 - X^2 + \Gamma_c = \lambda \int_X^\infty \frac{A_{\infty c}''}{(\xi - X)^{1/2}}\, \mathrm{d}\xi, \tag{5.2}$$

$$O(\sqrt{\Delta\Gamma}): \quad \left(2A_{\infty c} - \lambda \int_X^\infty \frac{\mathrm{d}\xi}{(\xi - X)^{1/2}} \frac{\partial^2}{\partial \xi^2}\right) \bar{a}_1 = 0, \tag{5.3}$$

$$O(\Delta\Gamma): \quad \bar{a}_1^2 + 2A_{\infty c}\bar{a}_2 - 1 = \lambda \int_X^\infty \frac{\mathrm{d}\xi}{(\xi - X)^{1/2}} \frac{\partial^2 \bar{a}_2}{\partial \xi^2} + \frac{\lambda}{2} \frac{\partial^2}{\partial \bar{Z}^2} \int_X^\infty \frac{\bar{a}_1\, \mathrm{d}\xi}{(\xi - X)^{1/2}}, \tag{5.4}$$

where we have used a new integration variable $\zeta = (\bar{Z} - \bar{\eta})/\Delta\Gamma^{1/4}$ instead of $\bar{\eta}$ and Taylor series expansion of the integrand about $\bar{Z}$. Here $\bar{Z} = \Delta\Gamma^{1/4}Z$ denotes the stretched coordinate in the spanwise direction and $a_1(X,\Delta\Gamma^{1/4}Z) = \bar{a}_1(X,\bar{Z})$. According to the assumption underlying the expansion (5.1) equation (5.2) simply represents the two-dimensional version of the solvability condition for the critical value Γ_c. Introducing abbreviations for the integral operators

$$I\cdot = \lambda \int_X^\infty \frac{1}{(\xi - X)^{1/2}} \frac{\partial^2 \cdot}{\partial \xi^2}\, \mathrm{d}\xi, \quad J\cdot = \lambda \int_X^\infty \frac{\cdot\, \mathrm{d}\xi}{(\xi - X)^{1/2}}, \tag{5.5}$$

equations (5.3) and (5.4) are recast in the form

$$(2A_{\infty c} - I)\bar{a}_1 = 0, \tag{5.6}$$

$$(2A_{\infty c} - I)\bar{a}_2 = 1 - \bar{a}_1^2 + \frac{1}{2} \frac{\partial^2}{\partial \bar{Z}^2} J\bar{a}_1. \tag{5.7}$$

From the second-order equation (5.6) we infer

$$\bar{a}_1(X,\bar{Z}) = b(X)c(\bar{Z}), \tag{5.8}$$

where $b(X)$ is the right eigenfunction corresponding to the eigenvalue 0 of the singular operator defined by (5.3),

$$(2A_{\infty c} - I)b = 0. \tag{5.9}$$

The shape function $c(\bar{Z})$ remains undetermined at this stage of approximation and has to be determined from the solvability condition of the third-order problem (5.7). To this end we introduce the left eigenfunction $n(X)$ of the operator $2A_{\infty c} - I$ defined by the corresponding adjoint operator

$$(2A_{\infty c} - I)^\dagger n := 2A_{\infty c} n - \lambda \frac{\mathrm{d}^2}{\mathrm{d}X^2} \int_{-\infty}^X \frac{n}{(X - \xi)^{1/2}}\, \mathrm{d}\xi = 0. \tag{5.10}$$

Using the notation

$$\langle n, q \rangle := \int_{-\infty}^\infty n(X) q(X)\, \mathrm{d}X \tag{5.11}$$

for functions q with $q(X \to \pm\infty) \to 0$ we obtain

$$\langle n, (2A_{\infty c} - I)\bar{a}_2 \rangle = 0. \tag{5.12}$$

Solutions to the third-order problem (5.7) therefore exist only if $c(\bar{Z})$ satisfies the 'evolution' equation

$$c'' - \alpha c^2 + \beta = 0, \tag{5.13}$$

where

$$\alpha = \frac{2\langle n, b^2 \rangle}{\langle n, Jb \rangle}, \quad \beta = \frac{2\langle n, 1 \rangle}{\langle n, Jb \rangle} \tag{5.14}$$

are real constants.

Physically acceptable solutions of (5.13) are expressed most conveniently in terms of the Jacobian elliptic functions $\mathrm{cn}(u|m)$, Abramowitz & Stegun (1970),

$$\frac{c(\bar{Z})}{c_s} = -\cos\varphi + \sqrt{3}\sin\varphi\left[1 - 2\,\mathrm{cn}^2\left(\sqrt{3\cos\varphi + \sqrt{3}\sin\varphi}\sqrt{\frac{\alpha c_s}{6}}\bar{Z}\,\middle|\,\frac{2\tan\varphi}{\sqrt{3}+\tan\varphi}\right)\right], \tag{5.15}$$

where $\pm c_s, c_s = \sqrt{\beta/\alpha}$ are the stationary points ($c' = 0$) of (5.13) corresponding to upper- and lower-branch solutions for planar flow; φ is an arbitrary constant within the range $[0, \pi/3]$, reflecting the infinite number of possible solutions of $c(\bar{Z})$ in the absence of a three-dimensional disturbance. It should be noted, however, that there exists in addition a singular solution of (5.13), which can be represented by the Weierstraß elliptic $\wp$-function in the form $c(\bar{Z})/c_s = 6\wp(\bar{Z})/\sqrt{\alpha\beta}$. Due to its unphysical behaviour this unbounded solution is discarded in the present investigation.

The homoclinic orbit of (5.13), i.e. the aperiodic limiting case of bounded solutions, is obtained by setting $\varphi = \pi/3$ in (5.15),

$$\frac{c(\bar{Z})}{c_s} = 1 - 3\cosh^{-2}\left(\sqrt{\frac{\alpha c_s}{2}}\bar{Z}\right). \tag{5.16}$$

Its asymptotic properties for large $|\bar{Z}|$ are given by

$$\frac{c(\bar{Z} \to \pm\infty)}{c_s} \sim 1 - 12\exp(-\sqrt{2\alpha c_s}|\bar{Z}|) + O(\exp(-2\sqrt{2\alpha c_s}|\bar{Z}|)) \tag{5.17}$$

and therefore reflect the rapidly decaying behaviour of the solutions corresponding to the upper branch as observed numerically. Furthermore, if (5.15) is expanded for small φ one obtains

$$\frac{c(\bar{Z})}{c_s} \sim -1 - \sqrt{3}\varphi\cos(\sqrt{2\alpha c_s}\bar{Z}) + O(\varphi^2), \quad \varphi \to 0, \tag{5.18}$$

expressing the periodic structure of the lower-branch solutions.

5.2. *Determination of $b(X)$ and the constants α and β*

The asymptotic results (5.17) and (5.18) indicate that

$$A(X,Z) \sim A_{\infty c}(X) + \sqrt{\Delta\Gamma}\,a_{1\infty}(X) + \Delta\Gamma\,a_{2\infty}(X) + \cdots + \exp(k_1\Delta\Gamma^{1/4}Z)(\sqrt{\Delta\Gamma}\,b(X) + \Delta\Gamma\,b_2(X) + \cdots) \tag{5.19}$$

represents a possible solution of (3.15) for $h \equiv 0$ in the limit $\Delta\Gamma \to 0$ with k_1 being a real or complex number. Herein $a_{1\infty}$ and $a_{2\infty}$ characterize the deviation of A from the critical shear stress distribution $A_{\infty c}$ for planar flow while the term containing the Z-dependence accounts for weak superimposed three-dimensional disturbances. By

substitution of (5.19) into (3.15) one obtains

$$O(\sqrt{\Delta\Gamma}): \quad (2A_{\infty c} - I)a_{1\infty} = (2A_{\infty c} - I)b = 0 \tag{5.20}$$

and therefore $a_{1\infty}(X) = c_1 b(X)$ with $c_1 = \text{const}$ in agreement with equation (5.8). Further, using this result and equating terms of $O(\Delta\Gamma)$ yields

$$(2A_{\infty c} - I)a_{2\infty} = 1 - c_1^2 b^2, \quad (2A_{\infty c} - I)b_2 = -2c_1 b^2 + \frac{k_1^2}{2} Jb. \tag{5.21}$$

The numerical solution procedure now is as follows. To determine $A_{\infty c}$, Γ_c, and $b(X)$, equation (3.21) is differentiated with respect to $A_\infty(0)$ to yield

$$(2A_\infty - I)\frac{\mathrm{d}A_\infty}{\mathrm{d}A_\infty(0)} + \frac{\mathrm{d}\Gamma}{\mathrm{d}A_\infty(0)} = 0. \tag{5.22}$$

Equations (3.21) and (5.22) were solved successively by means of a Newton iteration method with an initially prescribed $A_\infty(0)$ at the upper branch of the $A_\infty(0), \Gamma$ curve, figure 4, until the value of the derivative $\mathrm{d}\Gamma/\mathrm{d}A_\infty(0)$ reached zero to the desired accuracy. In this limit $A_\infty(X) \to A_{\infty c}(X)$, $\Gamma \to \Gamma_c \doteq 2.66$, and, as is seen by comparing equations (5.22) and (5.20), $\mathrm{d}A_\infty(X)/\mathrm{d}A_\infty(0) \to b(X)$. Since $b(0) = 1$, $b(X)$ is a unique function and, therefore, α and β are unique also, equations (5.14). Finally, c_1 and k_1^2 are determined uniquely in terms of α and β and as a consequence it is sufficient to calculate particular solutions of equations (5.21) by imposing e.g. the condition $a_{2\infty}(0) = 0$ and $b_2(0) = 0$ yielding in turn the desired result $c_1 \doteq \pm 0.878$ and $k_1^2 \doteq \pm 1.21$. From the relations $c_1 = \pm(\beta/\alpha)^{1/2} = \pm c_s$, $\alpha = k_1^2/(2c_1)$ and $\beta = k_1^2 c_1/2$ we finally deduce $\alpha \doteq 0.692$ and $\beta \doteq 0.533$.

Results showing the form of the functions $A_{\infty c}(X)$, $b(X)$, $a_{2\infty}(X)$, $b_2(X)$, and $c(\bar{Z})$ are depicted in figures 14 and 15. A comparison between numerical results and analytical predictions for lower-branch solutions is carried out in the final figure 16. Specifically we consider the variation of the wavenumber k characterizing the periodic flow pattern in the z-direction with $\Delta\Gamma$. The comparison strongly suggests that the values of $k^2/\sqrt{\Delta\Gamma}$ obtained numerically tend to the theoretical leading-order limit 1.21 for $\Delta\Gamma \to 0$. It also indicates that higher-order terms estimated to be of $O(\Delta\Gamma^{1/4})$ considerably influence the dependence of the wavenumber on $\Delta\Gamma$ except when $\Delta\Gamma$ is extremely small. The extension of the asymptotic theory presented here to higher order is currently under investigation.

6. Summary and conclusions

A numerical and analytical study of marginally separated flows past isolated obstacles on a locally flat plate has been performed. As in the case of strictly two-dimensional flow one has to distinguish between upper- and lower-branch solutions. In contrast to this case, however, these solutions are seen to exhibit qualitatively different properties if three-dimensional effects are accounted for. If an isolated hump is placed in an oncoming flow described by an upper-branch solution the resulting disturbances are as expected also localized, that is they rapidly decay in the stream and lateral directions on a scale B which characterizes the width of the hump. For $B \gg 1$ one recovers the quasi-two-dimensional results obtained earlier by Hackmüller & Kluwick (1989) which can be constructed from solutions of the two-dimensional version of the solvability condition. An approximate solution can also be obtained for slender humps $B \ll 1$ which predicts that the three-dimensional disturbances of the longitudinal component of the wall shear stress equals the local height of the

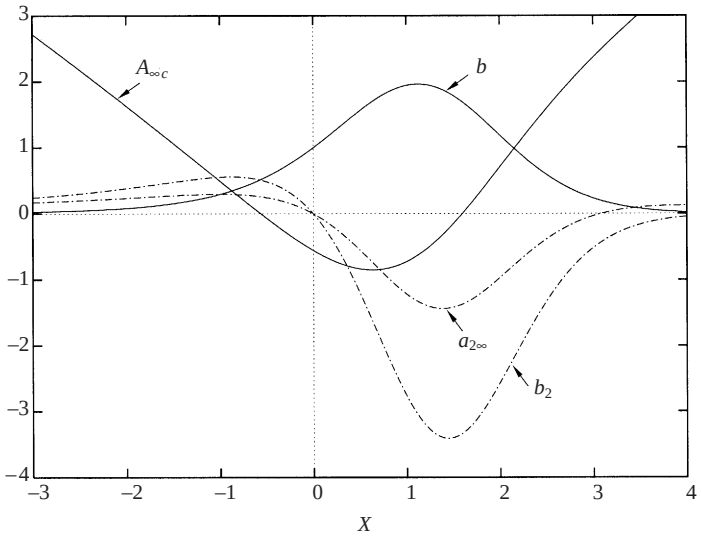

FIGURE 14. Leading-order term $A_{\infty c}(X)$ and correction $b(X)$ of the wall shear near the critical angle of attack Γ_c, equation (5.19).

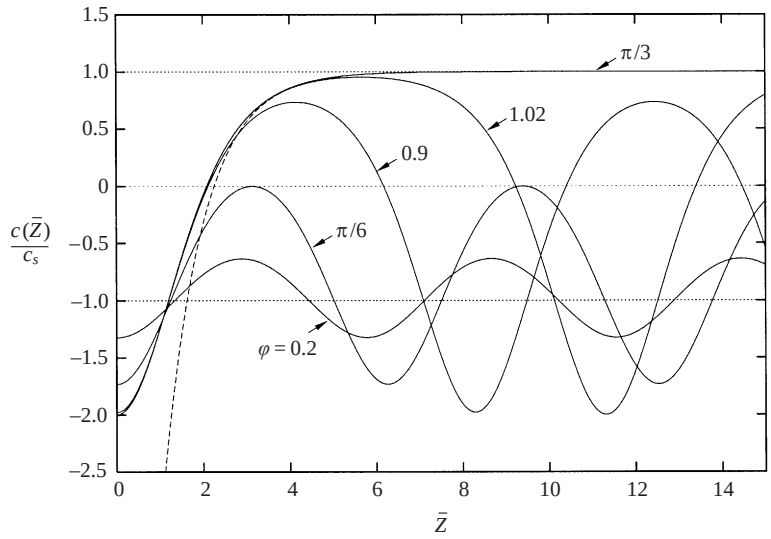

FIGURE 15. Variation of the wall shear in the spanwise direction, equation (5.15). Dotted lines: plane upper- and lower-branch solutions, dashed line: asymptote of homoclinic orbit for $\bar{Z} \to \infty$, (5.17).

obstacle. Slender humps, if sufficiently high are therefore an effective means to force reattachment of an oncoming marginally separated boundary layer locally.

Surprisingly, isolated obstacles are found to generate non-local disturbances if the oncoming two-dimensional flow is described by a lower-branch solution. Instead of generating perturbations which decay exponentially in the spanwise direction a periodic flow pattern is formed which extends up to infinity. The numerical results suggest that the wavelength is nearly independent of the width of the hump but depends on the difference of the parameter Γ and its critical value Γ_c beyond which no solution of purely two-dimensional flows past a locally flat wall exist. In

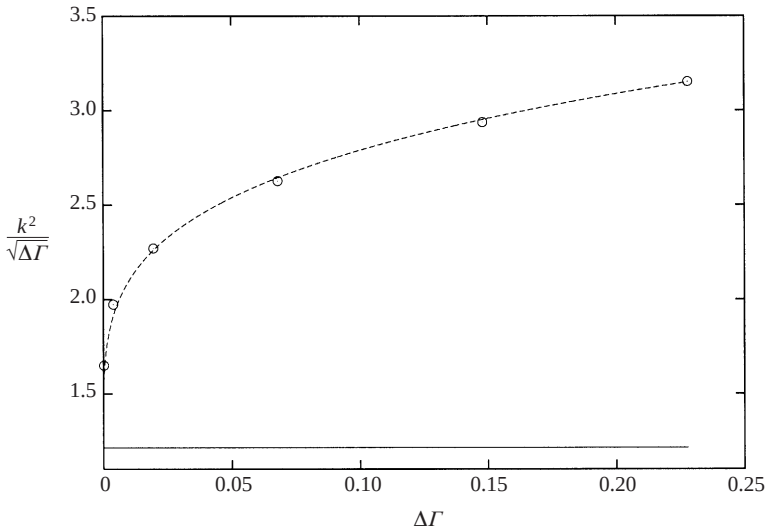

FIGURE 16. Comparison between numerical and asymptotic results concerning the wavenumber $k = |k_1|\Delta\Gamma^{1/4}$ of the periodic flow pattern in the limit $\Delta\Gamma \to 0$ (lower branch). Open circles denote numerical results for $H = 0.01$ ($H = 0.0001$ for the smallest value of $\Delta\Gamma$) and $B = 1$. Solid line: first-order solution (from equation (5.21), $k_1^2 = -1.21$), dashed line: curve fit $k^2/\sqrt{\Delta\Gamma} \sim 1.21 + 2.8\Delta\Gamma^{1/4}$.

addition the numerical investigations indicate that the amplitude associated with the periodic flow pattern tends to zero as $\Gamma_c - \Gamma \to 0$ and/or $B \to 0$ as well as $B \to \infty$. As a consequence, the flow behaviour near $\Gamma = \Gamma_c$ where the periodic flow behaviour branches off the exponentially decaying one can be studied analytically using asymptotic techniques. The applied method is closely related to methods used in the theory of weakly nonlinear waves and the resulting 'evolution equation' describing the variation of the flow field in the z-direction resembles the equation governing Stokes, cnoidal and solitary wave solutions of the Korteweg–de Vries equation. This in turn means that the resulting eigensolution describing weakly nonlinear three-dimensional disturbances on a locally flat wall are non-unique in the sense that the wavelength in the spanwise direction can be chosen arbitrarily within a semi-infinite interval. Comparison of numerical and analytical results shows good agreement. In passing we note that non-uniqueness of eigensolutions associated with three-dimensional interacting flows has also been observed in the different context of freely interacting supersonic boundary layers, Elliott, Rothmayer & Smith (1991).

Unfortunately, there seem to exist no experimental data on three-dimensional marginal separation to which the predictions of the present theory can be compared. One of these predictions is the waviness of the separation and attachment line associated with lower-branch solutions which follows immediately from the relationships (5.1) and (5.8) by setting the wall shear $A = 0$. One thus concludes that the shape of the separation and reattachment lines reflects the shape of the function c, see equation (5.15) and figure 15. According to figure 14 the value of $b(X)$ at the zeros of $A_{\infty c}$ differs by a factor of about 3. Therefore this effect is more pronounced at reattachment than at separation. Three-dimensional marginally separated flows with special emphasis on the transition to turbulence have recently been calculated by Alam & Sandham (2000) using direct numerical simulation. In their study a planar laminar boundary layer on a flat plate (Blasius type flow) encounters a region of

suction located at the outer edge of the boundary layer in order to force local boundary layer separation. A 'disturbance strip' in the form of imposed sinusoidal disturbances of the wall-normal velocity in time and in the spanwise direction which is located closely upstream of the suction region at the solid boundary finally results in a three-dimensional separation bubble. The separation line is clearly wavy and its shape is qualitatively similar to that of the prediction of the present work. Unfortunately, however, insufficient information is available to perform a rigorous comparison.

An obvious generalization of the results presented here is to include the effect of the hump shape into the bifurcation problem. Analytical work supplemented by more detailed numerical investigation of isolated but also periodic arrays of surface-mounted obstacles are carried out here. Also the first steps have been taken to study unsteady effects generated by impulsively generated or periodically oscillating flows. In this connection the interesting question arises of whether the 'evolution equation' derived here then becomes an evolution equation in the time sense, i.e. describing the propagation of weakly nonlinear waves in the transverse direction. Finally, it has to be clarified whether the bifurcation behaviour reported here is restricted to flows of boundary layer type or is characteristic of marginally separated flows in general. Preliminary results obtained for marginally separated jet flows indicate that the latter is true.

The authors would like to thank Professor H. Steinrück for useful suggestions and the referees for a number of helpful comments including in particular the alternative approach to equation (4.7). Also, discussions with Professor Ch. Schmeiser in the context of the 'Wissenschaftskolleg Partielle Differentialgleichungen' are gratefully acknowledged.

REFERENCES

Abramowitz, M. & Stegun, I. A. 1970 *Handbook of Mathematical Functions*, 7th Edn. Dover.

Alam, M. & Sandham, N. D. 2000 Direct numerical simulation of 'short' laminar separation bubbles with turbulent reattachment. *J. Fluid Mech.* **410**, 1–28.

Brown, S. N. 1985 Marginal separation of a three dimensional boundary layer on a line of symmetry. *J. Fluid Mech.* **158**, 95–111.

Brown, S. N. & Stewartson, K. 1983 On an integral equation of marginal separation. *SIAM J. Appl. Maths* **43**, 1119–1126.

Chernyshenko, S. I. 1985 On the asymptotics of stationary solutions of the Navier–Stokes equations at large Reynolds numbers. *Dokl. Akad. Nauk SSSR* **285**, 1353–1355.

Duck, P. W. 1989 Three-dimensional marginal separation. *J. Fluid Mech.* **202**, 559–575.

Elliott, J. W., Rothmayer, A. P. & Smith, F. T. 1991 The structure of three-dimensional free-interactions in external, steady, compressible flows. *Eur. J. Mech.* B/*Fluids* **10**, 227–251.

Elliott, J. W. & Smith, F. T. 1987 Dynamic stall due to unsteady marginal separation. *J. Fluid Mech.* **179**, 489–512.

Goldstein, S. 1948 On laminar boundary-layer flow near a position of separation. *Q. J. Mech. Appl. Maths* **1**, 43–69.

Hackmüller, G. & Kluwick, A. 1989 The effect of a surface-mounted obstacle on marginal separation. *Z. Flugwiss. Weltraumforsch.* **13**, 365–370.

Hackmüller, G. & Kluwick, A. 1991 Effects of 3-D surface-mounted obstacles on marginal separation. In *Separated Flows and Jets* (ed. V. V. Kozlov & A. V. Dovgal), pp. 55–65. Springer.

Hsiao, C.-T. & Pauley, L. L. 1994 Comparison of the triple-deck theory, interactive boundary layer method, and Navier–Stokes computation for marginal separation. *Trans. ASME: J. Fluids Engng* **116**, 22–28.

KLUWICK, A. 1998 Interacting laminar and turbulent boundary layers. In *Recent Advances in Boundary Layer Theory*. CISM courses and lectures No. 390 (ed. A. Kluwick), pp. 231–330. Springer.

KLUWICK, A. & REITERER, M. 1998 On three-dimensional marginal separation. *Z. Angew. Math. Mech.* **78**, S543–S544.

KLUWICK, A., REITERER, M. & HACKMÜLLER, G. 1997 Marginal separation caused by three-dimensional surface mounted obstacles. *Proc. 2nd Intl Conf. on Asymptotics in Mechanics, St. Petersburg 1996* (ed. A. H. Nayfeh & K. V. Rozhdestvensky), pp. 113–120. St. Petersburg State Marine Technical University.

RUBAN, A. I. 1981*a* Singular solution of boundary layer equations which can be extended continously through the point of zero surface friction. *Izv. Akad. Nauk SSSR: Mekh. Zhidk. Gaza* **6**, 42–52 (Engl. transl. *Fluid Dyn.* **16**, 835–843).

RUBAN, A. I. 1981*b* Asymptotic theory of short separation regions on the leading edge of a slender airfoil. *Izv. Akad. Nauk SSSR: Mekh. Zhidk. Gaza* **1**, 42–51 (Engl. transl. *Fluid Dyn.* **17**, 33–41).

SMITH, F. T. 2000 On physical mechanisms in two- and three-dimensional separations. *Phil. Trans. R. Soc. Lond.* A **358**, 3091–3111.

SMITH, F. T. & DANIELS, P. G. 1981 Removal of Goldstein's singularity at separation, in flow past obstacles in wall layers. *J. Fluid Mech.* **110**, 1–37.

SMITH, F. T., SYKES, R. I. & BRIGHTON, P. W. M. 1977 A two-dimensional boundary layer encountering a three-dimensional hump. *J. Fluid Mech.* **83**, 163–176.

STEWARTSON, K. 1970 Is the singularity at separation removable? *J. Fluid Mech.* **44**, 347–364.

STEWARTSON, K., SMITH, F. T. & KAUPS, K. 1982 Marginal separation. *Stud. Appl. Maths.* **67**, 45–61.

SYCHEV, V. V., RUBAN, A. I., SYCHEV, VIK. V. & KOROLEV, G. L. 1998 *Asymptotic Theory of Separated Flows*. Cambridge University Press.

VILENSKII, G. G. 1991 Three-dimensional local separation. *Izv. Akad. Nauk SSSR: Mekh. Zhidk. Gaza* **3**, 39–47 (Engl. transl. *Fluid Dyn.* **26**, 349–356).

ZAMETAEV, V. B. 1987 Local separation on a slender cone preceding the appearance of a vortex sheet. *Izv. Akad. Nauk SSSR: Mekh. Zhidk. Gaza* **6**, 21–28 (Engl. transl. *Fluid Dyn.* **22**, 842–848).